Neuro-Oncology
28(4), 911–922, 2026 | https://doi.org/10.1093/neuonc/noaf296 | Advance Access publication 29 December 2025

Distinct molecular profiles characterize the spontaneous growth rate of IDHmt low-grade astrocytomas and oligodendrogliomas

Amélie Darlix[†], Pierre Bady[†], Jérémy Deverdun, Emmanuelle Le Bars, Arthur Coget, Justine Meriadec, Mathilde Carrière, Hugues Duffau, and Monika E. Hegi

All author affiliations are listed at the end of the article

Corresponding Author: Monika E. Hegi, PhD, Lausanne University Hospital, Centre Hospitalier Universitaire Vaudois, Chemin des Boveresses 155, CLE-C 306, 1066 Epalinges, Switzerland (monika.hegi@chuv.ch).

[†]These two authors contributed equally.

Abstract

Background. The life expectancy of patients with diffuse IDH-mutant low-grade gliomas (IDHmt LGG) ranges from 5 to over 20 years. Tumor behavior, including spontaneous growth rate, varies even within homogeneously classified subtypes of oligodendroglioma and astrocytoma. Risk-adjusted treatment strategies are needed to avoid therapy-related toxicities without compromising outcome. The spontaneous tumor volume growth rate (TVGR) serves as a prognostic marker and predicts response to therapy. Accurate prediction of TVGR through biomarkers would enable improved evidence-based risk management.

Patients and Methods. A cohort of 77 patients treated in Montpellier, France, for IDHmt LGG grade II (WHO 2016) (29 oligodendrogliomas and 48 astrocytomas) was constituted (age >18 years; MRI scans, frozen tumor tissue). The DNA methylome (Illumina, EPIC array) and transcriptome (RNAseq) were established. TVGR was determined based on serial MRIs collected over the "watch & wait" period before the first treatment beyond surgery. Transcriptomic and methylome data were analyzed for signatures associated with TVGR using rank-rank regression followed by preranked gene set enrichment analysis.

Results. The median TVGR was lower in IDHmt codeleted compared to non-codeleted LGG (0.241 year^{-1} range 0.082-0.366 vs. 0.424 year^{-1} range 0.264-0.609, $P < .001$). In codeleted IDHmt LGG, TVGR was associated with upregulated gene signatures for neuronal systems, synaptic activity, and activation of repressed or poised signatures of neural progenitor cells, while the TVGR in non-codeleted IDHmt LGG was dominated by upregulated proliferation-related signatures, including DNA replication and repair.

Conclusion. Spontaneous TVGR of codeleted and non-codeleted IDHmt LGG involves distinct biological processes, suggesting possible differences in response to therapies.

Key Points

- IDHmt glioma WHO grade II growth rate impacts outcome and response to therapy.
- Molecular drivers of spontaneous growth rates are distinct between astrocytomas and oligodendrogliomas.
- Possible impact on treatment response and outcome.

Diffuse low-grade gliomas (LGG) WHO grade II are rare tumors with a yearly incidence of 1-2/10^5 that typically affect young patients before the age of 40. These tumors are characterized by a mutation in the isocitrate dehydrogenase (*IDH*) gene 1 or 2 (IDHmt) that is associated with a glioma CpG island methylator phenotype (G-CIMP) that affects expression of large sets

Received October 21, 2025; accepted December 28, 2025.

Importance of the Study

The life expectancy of patients with diffuse IDH-mutant low-grade gliomas (IDHmt LGG) WHO grade II ranges from 5 to over 20 years, with tumor behavior and growth rate varying even within homogeneous histo-molecular subtypes. Risk-adapted treatment strategies are needed to avoid therapy-related toxicities without compromising outcome. The spontaneous tumor volume growth rate (TVGR) is a prognostic marker and predicts therapy response. We analyzed a cohort of 77 patients with IDHmt LGG, with available MRI and tumor tissue. DNA methylome profiling and RNA sequencing were performed. TVGR was calculated from serial MRI during the "watch & wait" period before any treatment beyond surgery. TVGR in non-codeleted LGG patients was mainly associated with gene signatures linked with proliferation, while it was associated with upregulated gene signatures for signal transduction, neuronal systems, growth factor stimulation, and neural progenitors and stem cells in codeleted tumors. These insights suggest possible differences in response to therapies.

of genes. Although slowly growing, these tumors eventually progress to higher grade, with a median overall survival (OS) of 5 to over 20 years.[1] The prognosis depends on the genetic subtype in particular the presence of a codeletion of the chromosomal arms 1p and 19q (further referred to as codel), as well as clinical and radiological parameters such as tumor volume and spontaneous growth rate. Maximal safe surgical resection is the first-line treatment whenever possible, and the extent of resection has a positive prognostic impact.[1] However, the timing and choice of further treatments including systemic treatments (cytotoxic, targeted, or immunotherapies), radiation therapy (RT), or combinations thereof are debated. Depending on prognostic factors, a "watch & wait" strategy can be proposed following tumor resection in patients with a small residual volume. When clinical and/or radiologic criteria suggest progression, additional treatments (new surgery, systemic treatment, and/or RT) are initiated. The time interval between surgery/histological diagnosis and the initiation of the first medical treatment, beyond surgical resection, varies on a case-by-case basis, up to several years in selected cases. The growth rate of the tumor is a critical parameter to define the therapeutic treatment. It ranges from 1 to over 40 mm/year (median 4 mm/year) and has been shown to be an independent prognostic factor,[2] including in subgroups of molecularly defined tumors according to the 2016 WHO classification.[3,4] Lower growth rates have been observed in codel than in non-codel LGG.[5] The growth rate also has an impact on response to treatments (manuscript in preparation). To date, however, the mechanisms of the underlying biology are unknown due to a lack of associated molecular data.

We aimed at identifying molecular features associated with the tumor volume growth rate (TVGR) in a patient cohort constituted in a single institution (Montpellier, France) where the "watch & wait" strategy is usually proposed following tumor resection. The TVGR was established based on MRI data collected over the "watch and wait" period up to the time of initiation of the first oncologic treatment (beyond surgical resection) with the alkylating agent temozolomide (TMZ). To gain insights into the molecular underpinnings of the natural evolution of IDHmt LGG grade II, the tumor methylome (EPIC 850k methylation array) and transcriptome (RNA sequencing) were determined and analyzed, and associations with the TVGR were evaluated.

Methods

Patient Selection

A cohort of patients (≥18 years old) treated between 2002 and 2022 for a diffuse IDHmt low-grade (WHO 2016, grade II) glioma was constituted at the Institut régional du Cancer Montpellier (ICM) (BDD-NO database), France, as previously described.[6] In brief, selection criteria for patient inclusion comprised a confirmed histologic diagnosis of a diffuse IDHmt low-grade glioma grade II, according to the WHO 2016 classification, after review by an expert neuropathologist (Valērie Rigau),[7] TMZ as first-line oncologic treatment after surgery/ies, availability of frozen tumor tissue (biobanque, BB-0033-00059, CRB-ICM) and brain MRIs in *Digital Imaging and Communications in Medicine* (DICOM) format collected during the "watch & wait" period (MRI performed every 3 to 6 months) from first tumor diagnosis to the initiation of TMZ treatment as the first oncologic treatment beyond surgeries, defined as first intervention-free survival, FIFS. Treatment initiation was based on clinical (location, clinical symptoms) and radiological criteria (large postsurgical FLAIR tumor residue or tumor FLAIR volume progression). The standard treatment schedule was as follows: TMZ, day 1 to 5, every 28 days, 150 mg/m^2/day for the first cycle and 200 mg/m^2/day for the subsequent cycles as reported.[6] Tumor DNA methylome data (Illumina EPIC arrays) were available for 101 patients.

Patients' data were collected until September 19, 2025. All patients provided consent for translational research. The study was approved by the local Institutional Review Board (authorization #ICM-CORT-2019-2) and the ethics committee of the canton de Vaud (protocol CER-VD 2020-02519) in Lausanne, Switzerland.

Automated Determination of Tumor Volumes

MRI scans in DICOM format were collected. T1-weighted (T1w) and T2-FLAIR series were converted to NIfTI format and structured according to the Brain Imaging Data Structure (BIDS). Tumors were segmented using an automated procedure,[8] which has demonstrated good performance while significantly reducing the medical effort needed for

corrections. All segmentations were then visually reviewed by 3 experienced neuroradiologists (A.C., J.M., M.C.) and manually corrected if necessary, using the MRIcron software. The accuracy of the tumor margin definition has been thoroughly evaluated using the automated segmentation tool in a validation study as recently reported.[9] T2-FLAIR imaging and both anterior and posterior timepoints were used to maintain consistency across exams. Finally, each segmentation was rechecked by one of the 3 neuroradiologists who performed the corrections, ensuring that the reviewer was different from the one who initially checked the segmentation. The tumor volumes served as input to calculate the TVGR. The mean tumor diameter (MTD) was estimated from the tumor volume (mm^3) using the following formula: MTD (mm) = (2 × *V*)^(1/3). The first measurement entering the TVGR calculation corresponds to the first measure (immediate postoperative MRI excluded) of the tumor volume after initial resection at diagnosis or after the last resection before TMZ treatment for patients with multiple resections.

Modelling Tumor Growth and Estimation of the Growth Rate

The growth curves were fitted by a mixed linear model from the linearization of the exponential model for tumor volume and linear model for MTD. The model includes random intercept to take into account the lead-time bias (tumor sizes at the time of diagnosis) as proposed in Mandonnet et al.,[10] and a random slope to estimate the tumor progression for each patient. The model was completed by the subtype (1p/19q codeletion status) and interaction effect between subtype and time as fixed effects. The variance structure of within-group errors was modeled by a power variance function using covariates.[11]

The individual relative volume growth rate and linear diameter growth rate are given by the random and fixed slopes of the model and the coefficient related to interaction term.[12] A bootstrap procedure was used to consolidate the estimation of the relative TVGR and the linear MDT growth rate (TDGR) by the mean of the slopes from 50 repetitions and to provide confidence intervals of TVGR and TDGR. The tumor volume doubling time is defined as ln(2)/TVGR. The mixed models were provided by the function nlme from R package nlme.[11] The bootstrap of the mixed model was obtained by the function boot_lme from R package nlraa.[13]

DNA Methylome Analyses

Establishment of the methylome data (Illumina EPIC array) and respective preprocessing for the Montpellier cohort has been described previously.[6] The dataset is available under the GEO accession number GSE279950 (http://www.ncbi.nlm.nih.gov/geo/).

IDH Mutation Classification

Only IDH mutant tumors, confirmed using a methylome-based procedure[6,14] were retained for this study.

DNA Copy Number Assessment and 1p/19q Codeletion Status

DNA copy number assessments and determination of the 1p/19q codeletion status were performed using the DNA methylation data as described[6,15,16] using the combined intensities for methylated and unmethylated signals and circular binary segmentation to detect copy number aberration (CNA). The gene CNV states were provided by a clustering procedure using a mixture model yielding 5 CNA classes (a, amplification; g, gain; n, normal; d, hemizygous deletion; dd, homozygous deletion) from R package methyltools (https://github.com/badozor/methyltools).

MGMT Promoter Methylation

The DNA methylation status of the *MGMT* promoter (*MGMTp*) and the *MGMT* score (logit-transformed probability) were determined based on the EPIC data using the methylation probes, *cg12434587* and *cg12981137* and the logistic regression model MGMT-STP27 as previously described.[15,17] The Confidence Interval and MGMT classifications can directly be obtained by the function *MGMTpredict* from the R package mgmtstp27 for Inifinium platforms (27k, 450k, EPIC, and EPICv2, version 0.8, https://github.com/badozor/mgmtstp27).

Data Preparation and Analysis of RNA Sequencing

RNA was extracted from frozen tumor tissue using the AllPrep DNA/RNA Micro Kit (Qiagen, Cat. No./ID: 80284) as previously described.[6] RNA quality was assessed on a Fragment Analyzer (Agilent Technologies). The RNAs had RQNs between 6.3 and 9.7. The samples were randomized on a 96-well plate. RNA-seq libraries were prepared from 50 ng of total RNA with the Illumina Stranded mRNA Prep reagents (Illumina) using a unique dual indexing strategy and following the official protocol automated on a Sciclone liquid handling robot (PerkinElmer). Libraries were quantified by a fluorometric method (QubIT, Life Technologies) and their quality was assessed on a Fragment Analyzer (Agilent Technologies). Sequencing was performed on an Illumina NovaSeq 6000 S2 v1.5 flow cell for 100 cycles of single read. Sequencing data were demultiplexed using the bcl2fastq2 Conversion Software (version 2.20, Illumina). RNA sequencing was performed at the Lausanne Genomic Technologies Facility, Center for Integrative Genomics, University of Lausanne.

The preprocessing of RNAseq data was performed following the standard pipeline and recommendations from bcbio-nextgen (version 1.0.4, http://bcbio-nextgen.readthedocs.org/en/latest/). After trimming of adapter and polyA, and standard quality control, the alignments to the human reference genome (assembly GRCh37/hg19) were performed by hisat2 aligner (version 2.1.0). The gene expression data were summarized by trimmed mean of M-values (TMM) normalized counts (R package edgeR),[18,19] including log-transformation and using read counts and full library size. The Variant calling

analysis was performed with the software VarDict[20] and the genomic variant annotations were obtained by SNPeff.[21] Single nucleotide variants (SNVs) not passing the quality filter and silent and synonymous mutations were excluded. The genes listed in the COSMIC database as mutated in LGG and glioblastoma (GBM)[22] were used for our analysis. In addition, the identified SNVs were compared with the mutation database from TCGA for LGG and GBM (R package RTCGA.mutations). For personal privacy reasons, the RNA-seq raw data will be made available upon request.

External Datasets

External datasets comprised the grade II LGG dataset from The Cancer Genome Atlas characterized by IDH mutation predicted by the model from Yang et al.[14] after quality control and filtering (dbGaP accession number phs000178.v9.p8; http://cancergenome.nih. gov [23]). The TCGA dataset comprises 94 1p-19q non-codel and 80 codel patients.

Pathway Analyses

Association between markers (gene and CpG probes) and TVGR (and TDGR) was estimated by rank-rank regression.[24] The R package csranks provides statistical tools for estimation and inference involving ranks (the position in a ranking), and the function lmranks was used to perform rank-rank regression. The *z*-values from the regression provided the ranked gene lists usable for gene set enrichment analysis (GSEA).

Pathway analysis was performed by preranked GSEA-based Monte Carlo procedure (GSEA, R packages msigdbr and ClusterProfiler) using the Molecular Signatures Database (MSigDB, v7.5.1, updated 2022 collections of H hallmark gene sets and C2 curated gene sets).[25] The analyses were provided using a function from R package clusterprofiler.[26] Gene sets with Bonferroni-adjusted *P*-values ≤ .05 were considered significant. The averaged expression and DNA methylation for the selected pathway were weighted by their total inertia for the simultaneous heatmap representation as used in MFA (multiple factor analysis).[27] *The best k is selected according to the Calinski-Harabasz criterion from R package vegan.*[28] The annotations of the selected pathways were completed by a text mining procedure.

The selected pathways were described by additional annotation from Reactome (if available) and textual analysis (eg, pathway including the term "repair"). Pearson and Spearman correlations provide information on the strength and direction of the association between TVGR and the pathway (averaged expression or averaged DNA methylation).

The importance of the pathways in the prediction of the TVGR was individually estimated for each pathway by *r*-squared coefficient from the partial least square regression (PLS) of the TVGR on the gene expression (or DNA methylation probe).

Statistical Analyses

For the continuous variables, the Wilcoxon test (*t*) or Kruskal and Wallis test (*a*) was used to test the differences between 2 or more groups. The independence between qualitative variables and groups was tested with Pearson's chi-squared with Yates' continuity correction or based on permutation test.

The confidence intervals for proportion are given by exact binomial procedure (confidence level = 0.95). Survival univariate and multivariate models were computed by Cox proportional hazards regression model.[29] Analyses and graphical representations were performed using R-4.4.3 and the R package rms and survival (R2014, rms2014 and survival 2014). Similarity between matrices was evaluated by RV (vectorial correlation) coefficient (values between 0 and 1) ,[30] using R package ade4 for pairwise RV coefficient permutation tests[28] and computation of the MFA.[28]

Results

Patient Cohort

Tumor Growth Rate is Higher in Non-Codel than in Codel IDHmt LGG WHO Grade II.—A total of 88 patients (codel, *n* = 30; non-codel, *n* = 58) corresponding to 441 MRI scans in DICOM format over the "wait & watch" period up to the time of treatment initiation with TMZ (defined as First Intervention-Free Survival, FIFS) was initially selected (see sample flow in Supplementary Figure S1A). Among them, 78 also had matching molecular data. After excluding 1 patient with low QC data, 77 patients were included in the analyses (codel, *n* = 29; non-codel, *n* = 48). Their baseline characteristics are summarized in Table 1.

The determined tumor volumes served as input to calculate the tumor growth rate.

The median TVGR was lower in IDHmt codel LGG (oligodendroglioma) than for the non-codel (astrocytoma) as expected, 0.241 year^{-1} (range, 0.082 to 0.366) versus 0.424 year^{-1} (range, 0.264 to 0.609) (Figure 1, Table 2). The corresponding values for the TDGR are available in Table 2 and illustrated in Supplementary Figure S2. The correlation coefficient between the estimation of TVGR and TDGR was 0.95 (Spearman). The median tumor volume doubling time was 2.876 years (range 1.892 to 8.425) for codel and 1.636 years (range, 1.138 to 2.629) for non-codel. The quality of the model and the estimated TVGR are visualized in Supplementary Figure S3. Estimations of TVGR by patient are summarized in Supplementary Table S1, and respective information for the TDGR in Supplementary Table S2. No significant associations were observed between the TVGR and the tumor volume (mm^3) of the first MRI of the series by patient for non-codel or codel LGGs ($R = 0.24$, $P = .099$; $R = 0.053$, $P = .78$; Spearman; Supplementary Figure S4). This is in accordance with a previous study, reporting that the pre- and postoperative tumor growth rate did not change; concluding that surgery or the postoperative tumor residue did not impact the tumor growth rate in diffuse LGGs of WHO grade II.[31]

Distinct Sets of Molecular Pathways Are Associated with Increased TVGR in Non-Codel versus Codel IDHmt LGG.—For 77 of these patients with IDHmt LGG matching molecular data was available comprising the DNA methylome (Illumina EPIC, 850k) and the transcriptome RNAseq. The association between markers (gene transcripts; CpG-probes; copy number variation, CNV) and the TVGR by rank-rank regression

Table 1. Baseline description by LGG subtype, codel and non-codel

Variable	*N*	Codel *N*=29[a]	Non-Codel *N*=48[a]	*P*-value[b]
Median age at diagnosis	77	40 (34, 50)	33 (29, 39)	.003
Biological sex	77			.023
F		16 (55%)	14 (29%)	
M		13 (45%)	34 (71%)	
Tumor location				
Frontal	77	21 (72%)	31 (65%)	.5
Occipital	77	1 (3.4%)	3 (6.3)	>.9
Temporal	77	9 (31%)	21 (44%)	.3
Parietal	77	6 (21%)	8 (17%)	.7
Insular	77	7 (24%)	18 (38%)	.2
Basal Ganglia	77	0	1 (2.1%)	>.9
Corpus Callosum	77	2 (6.9%)	1 (2.1%)	.6
Surgery type at diagnosis	77			.6
Biopsy		2 (6.9%)	2 (4.2%)	
Surgical resection		27 (93%)	46 (96%)	
Extent of resection[c]	77			.6
Total		0 (0%)	3 (6.3%)	
Subtotal		20 (69%)	26 (54%)	
Partial		7 (24%)	15 (31%)	
Not Applicable		2 (6.9%)	3 (6.3%)	
Missing		0 (0%)	1 (2.1%)	
Performance status	77			.8
0		12 (41%)	19 (40%)	
1		17 (59%)	27 (56%)	
2		0 (0%)	2 (4.2%)	
Re-resection	77			.5
No re-resection		21 (72%)	31 (65%)	
Re-resection		8 (28%)	17 (35%)	
MRIs/patient	77	6 (3, 8)	4 (3, 5)	.005
Time from diagnosis to TMZ-trt, months[d]	77	53 (29, 70)	33 (20, 63)	.075
Median follow-up, months	77	133 (100, 151)	96 (65, 132)	.006
MGMT-STP27 score	77	3.61 (3.13, 4.68)	2.24 (0.69, 2.82)	<.001

[a]Median (Q1, Q3); *n* (%).
[b]Wilcoxon rank sum test; Pearson's chi-squared test; Wilcoxon rank sum exact test.
[c]EOR at diagnosis: Total, no FLAIR residual disease; Subtotal, FLAIR residual disease <10 cc; Partial resection, FLAIR >10 cc; Not Applicable (Biopsy).
[d]Abbreviations: MRI, magnetic resonance imaging; *N*, number; TMZ-trt, TMZ treatment.

yielded gene lists that served as input into the preranked GSEA using the Molecular Signatures Database[25] (see flow of analyses, Supplementary Figure S1B).

When analyzing codel (n=29) and non-codel (n=48) IDHmt LGG together for molecular associations with the TVGR, the main features of the extracted significant pathways characterized the subtype as determined by variation partitioning. A part was explained by the interaction of the subtype and the TVGR, while the variation explaining the growth rate was very low. This was true using either functional DNA methylation from promoter regions, gene expression (RNA-seq) or CNV (DNA methylation data derived) as illustrated in a heatmap (Supplementary Figure S5). This was not a surprising result, emphasizing that codel and non-codel IDHmt LGG are molecularly and biologically distinct diseases.

Subsequently the analyses were performed by subtype, non-codel and codel, separately, using the respective preranked gene lists as input. The resulting significant GSEA-derived pathways associated with the TVGR were summarized in heatmaps representing pathway activities, defined as mean expression levels of the respective genes by tumor sample (Figure 2A and B). The corresponding pathways are listed in Supplementary Tables S3 and S4 for non-codel and codel samples, respectively (gene expression, functional DNA methylation, and CNV). For non-codel IDHmt LGG, 219 gene signatures were found significantly associated with the TVGR. They were dominated by upregulation of proliferation-related signatures (cell cycle, DNA repair, DNA replication, and transcription) (Figure 2A, Supplementary Table S3). Pathways negatively correlated with the TVGR comprised neural subtype related (signature for neural GBM[32]) and markers for cell identity and differentiation, for example, neuronal differentiation. For the codel IDHmt LGG, 54 pathways were associated with the TVGR. The main

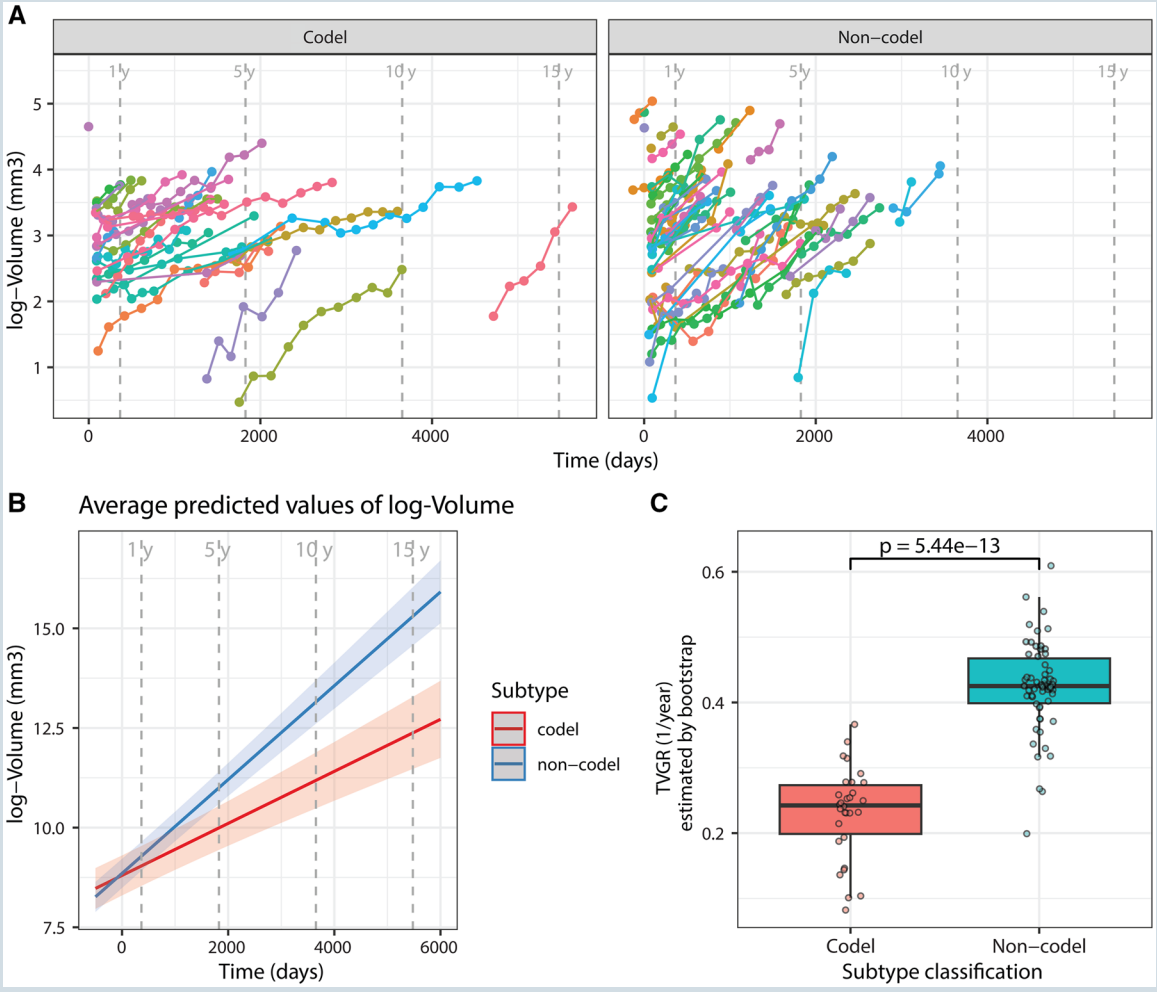

Figure 1. Tumor volume growth rate. (A) Representation of the tumor volume (mm^3) in function of time ($t=0$, time of diagnosis) by subtype (codel, $n=30$; non-codel, $n=58$). (B) Average predicted log volume by subtype, the shaded areas correspond to the 95% confidence interval. (C) Mean tumor volume growth rate (TVGR) estimated by bootstrap in codeleted and non-codeleted LGG, visualized in a Box plot as mean TVGR/year by subtype. The corresponding analyses with the tumor diameter growth rate (TDGR) are illustrated in Supplementary Figure S2.

Table 2. Tumor growth rate stratified by lgg subtype, codel and non-codel

Variable	*N*	Codel *N*=29[a]	Non-Codel *N*=48[a]	*P*-value[b]
TVGR, year^{-1}	77	0.24 (0.19, 0.26)	0.42 (0.40, 0.46)	<.001
TDGR, mm/year	77	2.88 (1.97, 3.41)	5.09 (4.57, 5.76)	<.001
TVDT, years	77	2.88 (2.65, 3.58)	1.64 (1.49, 1.75)	<.001

Abbreviations: *N*, number; TVGR, tumor volume growth rate; TDGR, tumor diameter growth rate; TVDT, tumor volume doubling time.
[a]Median (*Q*1, *Q*3).
[b]Wilcoxon rank sum exact test.

features of the selected pathways comprised upregulation of signatures for signal transduction, for example, across synapses, neurotransmitter receptors and postsynaptic signal transmission, neuronal systems, and growth factor stimulation (eg Nerve Growth Factor, NGF). Furthermore, upregulation of signatures that are epigenetically repressed or poised (eg signatures of PRC2 target genes[33]) and are related to development and differentiation of neural progenitor cells and stem cells.[34] For cell identity-related signatures upregulation of neuron markers and downregulation of oligodendrocyte markers were observed.[35] Downregulation was noted for signatures for mesenchymal GBM[32] and invasion[36] (Figure 2B).The top 30 up- or downregulated pathways of the non-codeleted and codeleted tumors are illustrated in

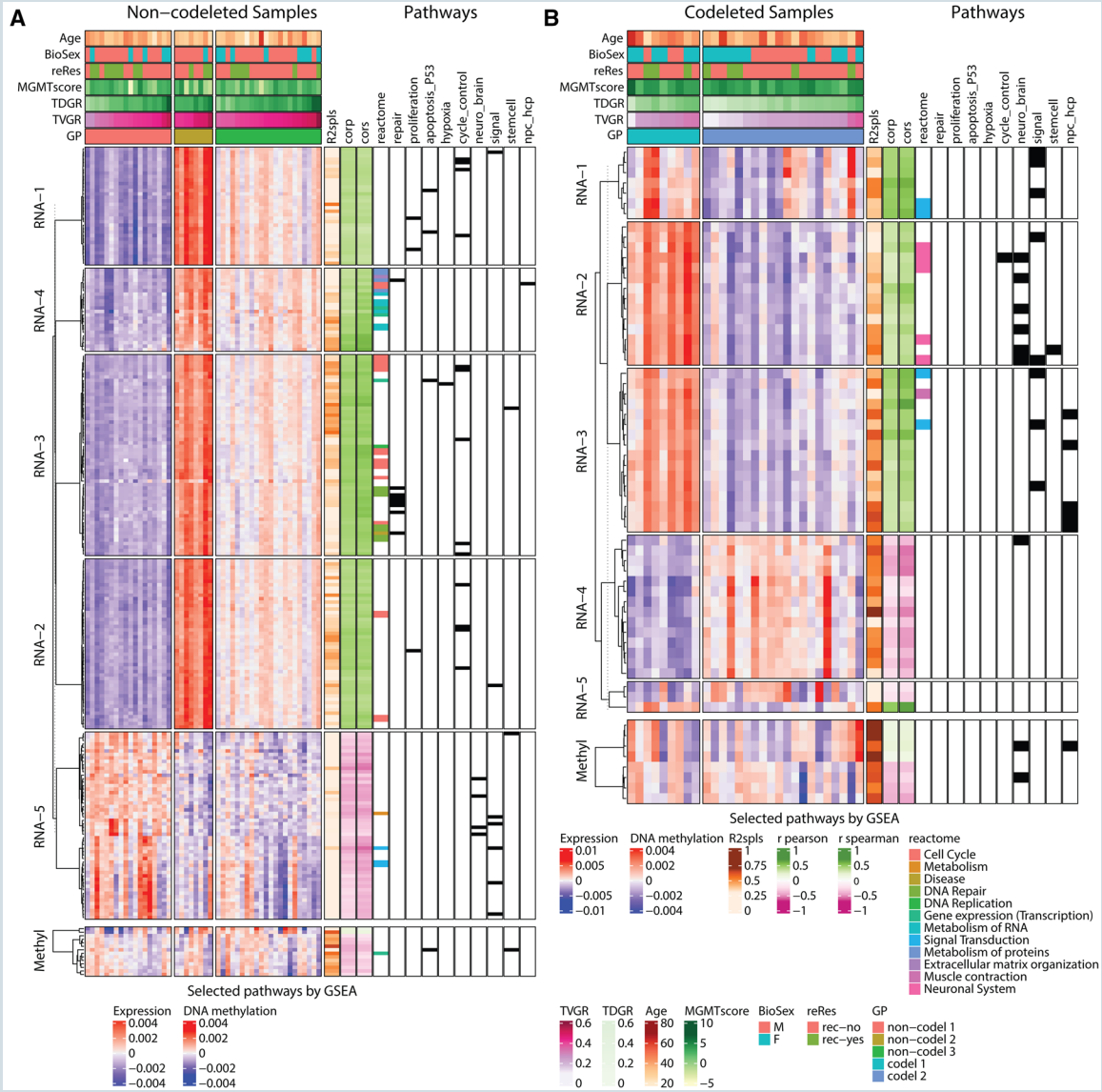

Figure 2. Pathways associated with TVGR for 1p/19q non-codeleted and codeleted IDHmt LGG. Pathways selected by GSEA for their associations with the estimated tumor volume growth rate (TVGR) before the oncologic treatment intervention (TMZ), illustrated in a heatmap by LGG subtype; non-codel (A) and codel (B). The respective gene expression and DNA methylation normalized datasets were weighted by their total inertia for the simultaneous heatmap representation, reflecting pathway activity, as used in multiple factor analysis (MFA) beforehand. The corresponding dendrograms are based on Euclidean distance and Ward's classification for the non-codeleted (A) and codeleted (B) datasets. Pathway annotations comprise the associations with the TVGR (R2spls, *r*-squared from SPLS [sparse partial least squares]); corp, Pearson's correlation; cors, Spearman's correlation. Further pathway annotations are illustrated with a color code for the reactom, and in black pathways selected for recurrent signatures. Sample annotations comprise the GP, molecular group partition; TVGR, TDGR, MGMT-STP27score; reRes, reresection(s); BiolSex, biological sex, and age at diagnosis.

ridge plots in Supplementary Figure S6. A small set of 11 pathways overlapped in the analyses of the 2 subtypes, comprising transcription factor and growth factor related pathways. However, for all 11 pathways the association with the respective TVGR was in the opposite direction, as illustrated in ridge plots (Supplementary Figure S7). A negative correlation was associated with 9 pathways in the non-codel, while they were positively correlated in the codel, and vice versa for the other 2 pathways. An invasion-related signature was upregulated in non-codel and downregulated in the codel.[37]

Few pathways were associated with functional methylation in both LGG subtypes. In the non-codel IDHmt LGG, pathways were dominated by negative correlation with DNA repair pathways (3/14) and oligodendrocyte markers or differentiation-associated pathways (3/14). In the codel IDHmt LGG, the functional methylation-selected pathways ($n=8$) comprised development and differentiation in the brain.

Few signatures emerged based on CNVs. Two signatures (of 9) in the non-codel tumors were positively correlated with the TVGR and reflected amplified regions on CHR

7Q21_22 and CHR 7P22 (known from breast cancer). Both signatures were also on the short list (2 of 4) for the codel group, but with the opposite (negative) correlation (Supplementary Tables S3 and S4).

Transcriptome-based Prediction of Tumor Growth Rate and Outcome .—Next, we aimed at identifying tumor subgroups with distinct pathway activities explaining the TVGR. For non-codel IDHmt LGG, partitions into 3 molecular subgroups were proposed and 2 for the codel (K-means partitioning using Calinski criterion to detect the optimal partition)[38] (Figure 2A and B, Supplementary Figure S8). In both the non-codel and the codel IDHmt tumors, the association of the group partition (GP) with the TVGR was significantly different (Figure 3A and B). The corresponding Kaplan–Meier analysis testing the GP with outcome suggested for the non-codel a significant difference for the FIFS (P=.018, log-rank, Figure 3C) and a significant difference for OS (Supplementary Table S5). For the codel IDHmt LGG cohort, no difference (P=.36, log-rank) was observed for the association of the GP and FIFS (Figure 3D) (Supplementary Table S5). However, the small sample size of the subgroups precludes any strong statement (n=9, n=20).

The direct association of the TVGR with FIFS was significant in the non-codel patient cohort (P=.019) and also significant for OS (Supplementary Table S6). In the codel patients, the direct association of the TVGR with FIFS did not reach significance (P=.130). The OS data are immature for the codel patients (79% alive, 23/29). Of note, the TVGR was significantly associated with PFS after TMZ treatment, defined as the time interval from TMZ treatment initiation to the next treatment for non-codel and codel patients. Outcome measures in association with the GP and the TVGR are summarized in Supplementary Tables S5 and S6, respectively.

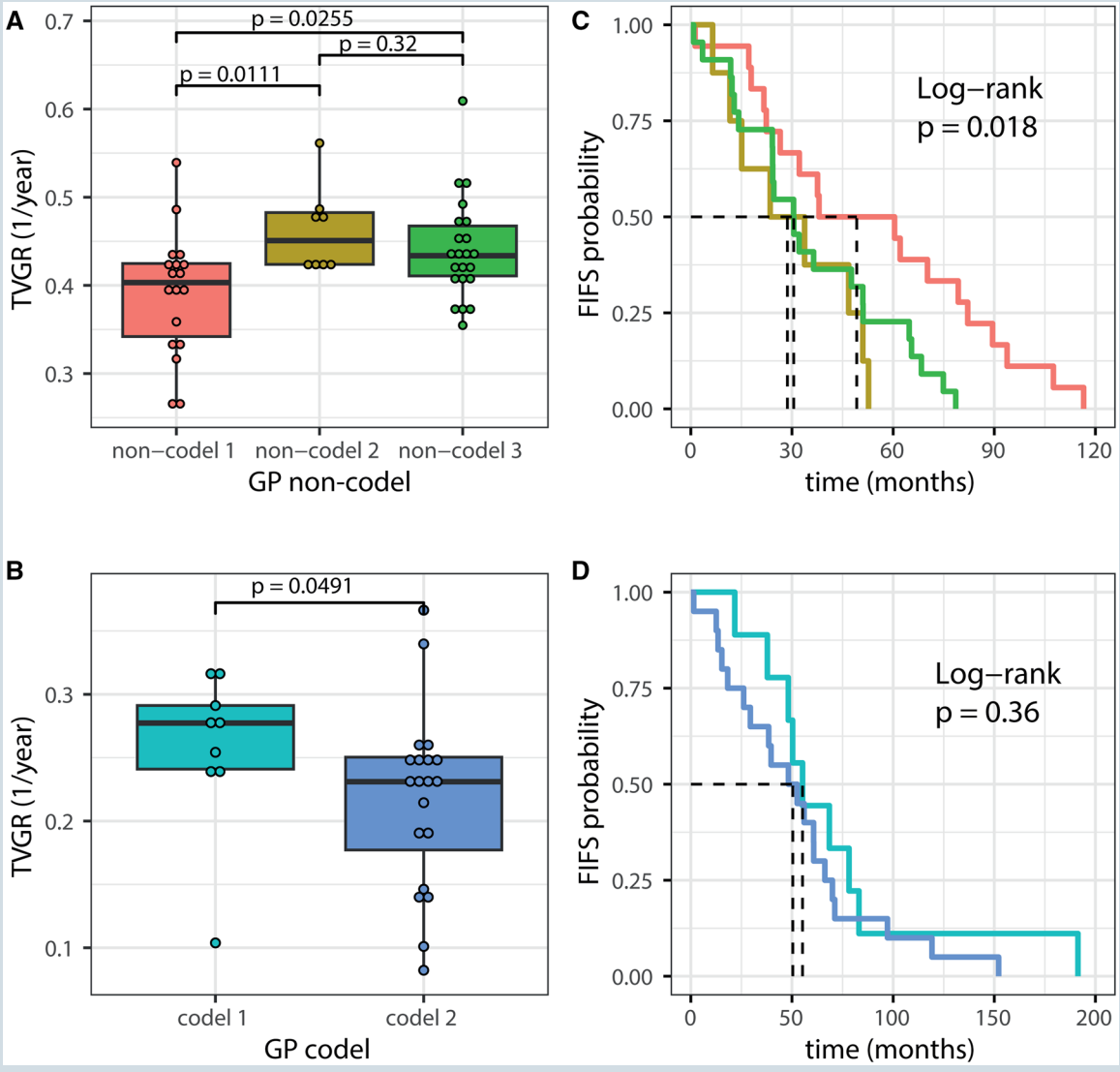

Figure 3. Association of molecular subgroups with first-intervention-free survival (FIFS). Boxplot representation of TVGR in function of the molecular subgroups (GP, group partitions) defined by cascade K-means of pathway expression for non-codeleted (A) and codeleted (B) patients. The association between FIFS and the GP groups is represented by Kaplan–Meier plot and tested by log-rank test for non-codeleted (C) and codeleted (D) patients.

Patients with re-resections were not enriched in any of the molecular subgroups in either of the 2 glioma subtypes, non-codel or codel (Figure 2A and B, Fisher's Exact test, $P = .5192$ for non-codel and $P = .6749$ for codel).

Evaluation of TVGR Related Signatures in the TCGA-LGG (IDHmt, Grade II) Dataset.—We determined the TVGR-associated expression and methylation signatures extracted in this study in the TCGA-LGG IDHmt, grade II samples ($n = 174$), stratified by the codel status. Comparison to the respective data structures in the Montpellier dataset showed high similarity, as illustrated in a heatmap in Supplementary Figure S9. The respective similarity measures were high, with RV coefficients of 0.91 for the expression signatures in the non-codel and 0.83 for the codel subpopulations. Similarly, the methylation-based signatures exerted high RV coefficients of 0.93 and 0.92 in non-codel and codel, respectively (Supplementary Figure S9E-H). *P*-values are .01 with 99 repetitions for all comparisons.

(Epi)Genetic Alterations.—We tested the presence of (epi) genetic alterations reported to be associated with progression to higher tumor grade or malignant progression after treatment.[39–43] None of the tumor samples displayed a G-CIMP-low phenotype. Evaluation of CNVs at a set of genes reported to be relevant for astrocytic glioma progression and worse outcome when homozygously deleted or amplified,[39] revealed only one non-codel IDHmt LGG with a homozygous deletion of *CDKN2A/B* and one with amplification of *CDK6.* Otherwise, few samples showed hemizygous deletions at genes such as *CDKN2A/B, RB1*, or *MGMT* (Supplementary Figure S10). This CNV pattern with rare homozygous deletions or amplifications at key glioma-relevant genes, is in accordance with the selection criteria of WHO 2016 grade II and with one exception also grade II according to CNS5 WHO 2021. Mutation analyses using the RNA-seq data, for mutations reported relevant in IDHmut LGG, showed a good concordance for *IDH1*or *2* mutations. The next most commonly mutated gene was *TP53*, followed by mutations in *PIK3CA* and *PIK3R1*. Other mutations were rare (Supplementary Figure S8). *ATRX* mutations were underreported; however, RNA-based mutation analyses have limited sensitivity as they depend on transcript levels.

Discussion

In patients with IDHmt gliomas grade II, tumor behavior is heterogeneous within homogeneous subtypes of tumors according to the WHO 2016 classification, in terms of outcome and spontaneous growth rate.[3,4] In this study we confirm that the growth rate is negatively associated with survival[2] and response to TMZ treatment (manuscript in preparation). In this context, understanding its biological correlates is of upmost importance, to adapt the treatment strategy at the individual level. In this study, we aimed at identifying molecular features associated with the spontaneous TVGR in a cohort of patients diagnosed with IDHmt non-codel and codel LGG, to uncover, and maybe, in the near future, act upon molecular characteristics that are associated with increased growth rate. The TVGR was established based on MRI data collected over the "wait & watch" period from tumor diagnosis up to the time of treatment initiation with TMZ (FIFS). The median TVGR was lower in IDHmt codel LGG (oligodendroglioma) than the non-codel (astrocytoma) as expected.[5]

[44] The TVGR per se had a significant association with FIFS in the IDHmt non-codel patient cohort and a borderline significant association in the IDHmt codel cohort.

Insights into the molecular analyses revealed that gene signatures associated with the TVGR were dominated by upregulation of proliferation-related pathways, such as cell cycle, DNA repair, DNA replication, and transcription in the non-codel IDHmt LGG. Respective expression profiles suggested 3 distinct molecular patient subgroups that were significantly associated with FIFS, response to TMZ, and OS. Upregulation of the signatures was associated with worse outcome.

In codel IDHmt LGGs, the association of the transcriptome with the TVGR yielded different deregulated sets of gene signatures reflecting multiple pathways, such as upregulation of signatures for signal transduction (eg, across synapses), neuronal systems, growth factor stimulation, and differentiation-related signatures of neural progenitor cells and stem cells, but not proliferation-related signatures. This may suggest that the TVGRs of the spontaneous evolution of non-codel and codel IDHmt LGG are associated with and driven by distinct biological processes that may imply differences in their response to specific therapies. We could confirm the identified molecular signatures associated with the TVGR in the Montpellier cohorts in TCGA-LGG (grade II) dataset for the IDHmt non-codel and codel LGGs, respectively. In this context, it is noteworthy that an IDHmt-targeted drug, which reduces the production of the oncometabolite 2-hydroxy glutarate, influenced the lineage differentiation state of tumor cells in IDHmt codel LGG of patients who responded to the drug. At the time of tumor resection, these patients had been undergoing treatment for 4 weeks as part of a phase I clinical trial with the mutant IDH1/2 inhibitor ivosidenib.[45] It may be speculated that mutant IDH inhibitors may epigenetically reprogram the tumors, thereby downregulating the pathways we observed activated in association with an increased TVGR in the codel IDHmt LGG. This would be in accordance with their reported slowed growth.

There are some limitations to this study. While we were able to validate the gene signatures in the TCGA-LGG cohorts, we could not evaluate the association with growth rate and outcome. The patients in the Montpellier cohort were selected to evaluate the spontaneous TVGR during the "watch & wait" period, from diagnosis to initiation of any oncologic treatment (apart surgery), defined as first intervention-free survival (FIFS). By definition of the inclusion criteria, all patients included reached this event. This contrasts with the outcome information available for patients in the IDHmt grade II TCGA-LGG cohort, where the proportion of events and definition of a progression free interval (PFI, time from diagnosis to the occurrence of any new tumor event) is different, 0.56 (34 of 60) for non-codel and 0.23 (15 of 65) for codel.[46] Therefore, outcome data are not directly comparable and the association of the molecular profiles with the FIFS cannot be validated and warrants further studies.

Taken together, the TVGR of the spontaneous evolution of non-codel IDHmt and codel LGG is associated with distinct biological processes. This implies that they may respond differentially to therapies. Insights into the biological

mechanisms associated with the tumor growth rate may facilitate risk-optimized choices, together with clinical parameters, such as tumor location and size, and patient preference, when additional treatments are required.

Supplementary Material

Supplementary material is available online at *Neuro-Oncology* (https://academic.oup.com/neuro-oncology).

Keywords

IDHmt diffuse LGG WHO grade II | molecular signatures | tumor volume growth rate

Author Contributions

Conception and design: M.E.H, A.D., P.B., and J.D. Acquisition of data (patient data, review of radiology): A.D., E.L.B., J.M., M.C., A.C., and H.D.). Analysis and interpretation of data (eg, statistical analysis, biostatistics, and computational analysis): M.E.H., P.B., and A.D. Manuscript writing: M.E.H., P.B., and A.D. Review and/or revision of the manuscript: all coauthors. Study supervision: M.E.H. and A.D.

Conflict of Interest Statement

A.D. has received honoraria for advisory board participation from the following for-profit companies: Novocure and Servier Pharmaceuticals. All other authors report no competing conflict of interest.

Funding

This study was funded by The Brain Tumour Charity (CB_2019/1_10398, GN-000682 to M.E.H. and A.D.); the Swiss Cancer Research Foundation (KFS-5555-02-2022 to M.E.H.); and the Swiss National Science Foundation (320030_215718 to M.E.H.).

Acknowledgments

Many thanks to the Biobanking Laboratory and the Molecular Biology Laboratory at the Institute of Pathology at the Lausanne University Hospital for ribonucleic acid extraction and the Lausanne Genomic Technologies Facility, Center for Integrative Genomics, University of Lausanne for RNA sequencing. This work has benefited from the facilities and expertise of the CRB Collection (NEUROLOGIE) of the University Hospital of Montpellier, France (www.chu-montpellier.fr). The results presented here are in part based upon data generated by the TCGA Research Network: https://www.cancer.gov/tcga.

Ethics Statement

All patients provided consent for translational research. The study was approved by the local Institutional Review Board of the Institut régional du Cancer Montpellier (ICM) (authorization #ICM-CORT-2019-2) France, and the ethics committee of the canton de Vaud (protocol CER-VD 2020-02519) Lausanne, Switzerland.

Data Availability

Due to privacy reasons the RNA sequencing data will be made available upon reasonable request under a Data Transfer Agreement. The methylome data from the Montpellier cohort are available under the GEO accession number GSE279950 (https://www.ncbi.nlm.nih.gov/geo/query/acc.cgi? acc=GSE279950). The external datasets used comprised methylome and RNA sequencing (Level 3) data from the LGG dataset of The Cancer Genome Atlas dbGaP accession number phs000178.v9.p8; http://cancergenome.nih.gov).

Affiliations

Department of Medical Oncology, Institut Régional du Cancer de Montpellier, University of Montpellier, Montpellier, France (A.D.); Institute of Functional Genomics (IGF), University of Montpellier, CNRS, INSERM, Montpellier, France (A.D.); Neuroscience Research Center and Service of Neurosurgery, Lausanne University Hospital and University of Lausanne, Lausanne, Switzerland (P.B., M.E.H.); Translational Data Science Facility, Swiss Institute of Bioinformatics, AGORA Cancer Research Centre, Lausanne, Switzerland (P.B.); I2FH, Institut d'Imagerie Fonctionnelle Humaine, Department of Neuroradiology, Montpellier University Medical Center, Montpellier, France (J.D., E.L.B.); Department of Neuroradiology, Gui de Chauliac Hospital, Montpellier University Medical Center, Montpellier, France (J.D., E.L.B., A.C., J.M., M.C.); Department of Neurosurgery, Gui de Chauliac Hospital, Montpellier University Medical, Montpellier, France (H.D.); L. Lundin and Family Brain Tumor Research Center, Departments of Oncology and Clinical Neurosciences, Lausanne University Hospital and University of Lausanne, Lausanne, Switzerland (M.E.H.)

References

1. Ng S, Rigau V, Moritz-Gasser S, et al. Long-term autonomy, professional activities, cognition, and overall survival after awake functional-based surgery in patients with IDH-mutant grade 2 gliomas: a retrospective cohort study. *Lancet Reg Health Eur.* 2024;46:101078. https://doi.org/10.1016/j.lanepe.2024.101078
2. Pallud J, Blonski M, Mandonnet E, et al. Velocity of tumor spontaneous expansion predicts long-term outcomes for diffuse low-grade gliomas. *Neuro Oncol.* 2013;15:595–606. https://doi.org/10.1093/neuonc/nos331
3. Roux A, Tauziede-Espariat A, Zanello M, et al. Imaging growth as a predictor of grade of malignancy and aggressiveness of IDH-mutant and

1p/19q-codeleted oligodendrogliomas in adults. *Neuro Oncol*. 2020;22:993–1005. https://doi.org/10.1093/neuonc/noaa022

4. Leclerc A, Roux A, Elia A, et al. Radiographic growth rate as a predictor of aggressiveness of diffuse gliomas without 1p19q codeletion. *Neurosurg Focus*. 2024;56:E4. https://doi.org/10.3171/2023.11.FOCUS23648
5. Huang RY, Young RJ, Ellingson BM, et al. Volumetric analysis of IDH-mutant lower-grade glioma: a natural history study of tumor growth rates before and after treatment. *Neuro Oncol*. 2020;22:1822–1830. https://doi.org/10.1093/neuonc/noaa105
6. Darlix A, Bady P, Deverdun J, et al. Clinical value of the MGMT promoter methylation score in IDHmt low-grade glioma for predicting benefit from temozolomide treatment. *Neurooncol Adv*. 2025;7:vdae224. https://doi.org/10.1093/noajnl/vdae224
7. DN Louis, H Ohgaki, OD Wiestler, et al., eds. *WHO Classification of Tumours of the Central Nervous System*. Revised 4th ed. Lyon: IARC; 2016.
8. Verdier M, Deverdun J, de Champfleur NM, et al. Evaluation of a nnU-Net type automated clinical volumetric tumor segmentation tool for diffuse low-grade glioma follow-up. *J Neuroradiol*. 2024;51:16–23. https://doi.org/10.1016/j.neurad.2023.05.008
9. Deverdin J, Clain G, Verdier M, et al. Beyond proof-of-concept: validating robust automated diffuse lower-grade glioma segmentation for clinical applications in longitudinal follow-up. *Neurooncol Adv*. 2025. https://doi.org/10.1093/noajnl/vdaf256
10. Mandonnet E, Delattre JY, Tanguy ML, et al. Continuous growth of mean tumor diameter in a subset of grade II gliomas. *Ann Neurol*. 2003;53:524–528. https://doi.org/10.1002/ana.10528
11. Pinheiro JC, Bates DM. *Mixed-Effects Models in S and S-plus*. 2000 ed. New York: Springer Verlag; 2000.
12. Heesterman BL, Bokhorst JM, de Pont LMH, et al. Mathematical models for tumor growth and the reduction of overtreatment. *J Neurol Surg B Skull Base*. 2019;80:72–78. https://doi.org/10.1055/s-0038-1667148
13. Archontoulis SV, Miguez FE. Nonlinear regression models and applications in agricultural research. *Agron J*. 2015;107:786–798. https://doi.org/10.2134/agronj2012.0506
14. Yang J, Wang Q, Zhang ZY, et al. DNA methylation-based epigenetic signatures predict somatic genomic alterations in gliomas. *Nat Commun*. 2022;13:4410. https://doi.org/10.1038/s41467-022-31827-x
15. Bady P, Delorenzi M, Hegi ME. Sensitivity analysis of the MGMT-STP27 model and impact of genetic and epigenetic context to predict the MGMT methylation status in gliomas and other tumors. *J Mol Diagn*. 2016;18:350–361. https://doi.org/10.1016/j.jmoldx.2015.11.009
16. Bady P, Kurscheid S, Delorenzi M, et al. The DNA methylome of DDR genes and benefit from RT or TMZ in IDH mutant low-grade glioma treated in EORTC 22033. *Acta Neuropathol*. 2018;135:601–615. https://doi.org/10.1007/s00401-018-1810-6
17. Bady P, Sciuscio D, Diserens AC, et al. MGMT methylation analysis of glioblastoma on the Infinium methylation BeadChip identifies two distinct CpG regions associated with gene silencing and outcome, yielding a prediction model for comparisons across datasets, tumor grades, and CIMP-status. *Acta Neuropathol*. 2012;124:547–560. https://doi.org/10.1007/s00401-012-1016-2
18. Robinson MD, Oshlack A. A scaling normalization method for differential expression analysis of RNA-seq data. *Genome Biol*. 2010;11:R25. https://doi.org/10.1186/gb-2010-11-3-r25
19. Robinson MD, McCarthy DJ, Smyth GK. edgeR: a bioconductor package for differential expression analysis of digital gene expression data. *Bioinformatics*. 2010;26:139–140. https://doi.org/10.1093/bioinformatics/btp616
20. Lai Z, Markovets A, Ahdesmaki M, et al. VarDict: a novel and versatile variant caller for next-generation sequencing in cancer research. *Nucleic Acids Res*. 2016;44:e108. https://doi.org/10.1093/nar/gkw227
21. Cingolani P, Platts A, Wang Le L, et al. A program for annotating and predicting the effects of single nucleotide polymorphisms, SnpEff: SNPs in the genome of Drosophila melanogaster strain w1118; iso-2; iso-3. *Fly (Austin)*. 2012;6:80–92. https://doi.org/10.4161/fly.19695
22. Tate JG, Bamford S, Jubb HC, et al. COSMIC: the catalogue of somatic mutations in cancer. *Nucleic Acids Res*. 2019;47:D941–D947. https://doi.org/10.1093/nar/gky1015
23. Brat DJ, Verhaak RG, Aldape KD, et al. Comprehensive, integrative genomic analysis of diffuse lower-grade gliomas. *N Engl J Med*. 2015;372:2481–2498.
24. Chetverikov D, Wilhelm D. Inference for Rank-Rank regressions. *ArXiv*. 2024. https://doi.org/10.48550/arXiv.2310.15512
25. Subramanian A, Tamayo P, Mootha VK, et al. Gene set enrichment analysis: a knowledge-based approach for interpreting genome-wide expression profiles. *Proc Natl Acad Sci U S A*. 2005;102:15545–15550. https://doi.org/10.1073/pnas.0506580102
26. Xu S, Hu E, Cai Y, et al. Using clusterProfiler to characterize multiomics data. *Nat Protoc*. 2024;19:3292–3320. https://doi.org/10.1038/s41596-024-01020-z
27. Escofier B, Pagès J. Multiple factor analysis (AFMULT package). *Computational Statistics & Data Analysis*. 1994;18:121–140. https://doi.org/10.1016/0167-9473(94)90135-X
28. Chessel D, Dufour AB, Thioulouse J. The ade4 package-I: one-table methods. *R News*. 2004;4:5–10.
29. Therneau TM, Grambsch PM. *Modeling Survival Data: Extending the Cox Model*. New York: Springer; 2000.
30. Escoufier Y. Le traitement des variables vectorielles. *Biometrics*. 1973;29:751–760. https://doi.org/10.2307/2529140
31. Mandonnet E, Pallud J, Fontaine D, et al. Inter- and intrapatients comparison of WHO grade II glioma kinetics before and after surgical resection. *Neurosurg Rev*. 2010;33:91–96. https://doi.org/10.1007/s10143-009-0229-x
32. Verhaak RG, Hoadley KA, Purdom E, et al. Integrated genomic analysis identifies clinically relevant subtypes of glioblastoma characterized by abnormalities in PDGFRA, IDH1, EGFR, and NF1. *Cancer Cell*. 2010;17:98–110. https://doi.org/10.1016/j.ccr.2009.12.020
33. Ben-Porath I, Thomson MW, Carey VJ, et al. An embryonic stem cell-like gene expression signature in poorly differentiated aggressive human tumors. *Nat Genet*. 2008;40:499–507. https://doi.org/10.1038/ng.127
34. Mikkelsen TS, Ku M, Jaffe DB, et al. Genome-wide maps of chromatin state in pluripotent and lineage-committed cells. *Nature*. 2007;448:553–560. https://doi.org/10.1038/nature06008
35. Lein ES, Hawrylycz MJ, Ao N, et al. Genome-wide atlas of gene expression in the adult mouse brain. *Nature*. 2007;445:168–176. https://doi.org/10.1038/nature05453
36. Schuetz CS, Bonin M, Clare SE, et al. Progression-specific genes identified by expression profiling of matched ductal carcinomas in situ and invasive breast tumors, combining laser capture microdissection and oligonucleotide microarray analysis. *Cancer Res*. 2006;66:5278–5286. https://doi.org/10.1158/0008-5472.CAN-05-4610
37. Poola I, DeWitty RL, Marshalleck JJ, Bhatnagar R, Abraham J, Leffall LD. Identification of MMP-1 as a putative breast cancer predictive marker by global gene expression analysis. *Nat Med*. 2005;11:481–483. https://doi.org/10.1038/nm1243
38. Caliński T, Harabasz J. A dendrite method for cluster analysis. *Communications in Statistics*. 1974;3:1–27.
39. Shirahata M, Ono T, Stichel D, et al. Novel, improved grading system(s) for IDH-mutant astrocytic gliomas. *Acta Neuropathol*. 2018;136:153–166. https://doi.org/10.1007/s00401-018-1849-4

40. Malta TM, de Souza CF, Sabedot TS, et al. Glioma CpG island methylator phenotype (G-CIMP): biological and clinical implications. *Neuro Oncol*. 2018;20:206–230.

41. Malta TM, Sabedot TS, Morosini NS, et al. The epigenetic evolution of glioma is determined by the IDH1 mutation status and treatment regimen. *Cancer Res*. 2024;84:741–756. https://doi.org/10.1158/0008-5472.CAN-23-2093

42. Ghisai SA, van Hijfte L, Vallentgoed WR, et al. Epigenetic landscape reorganisation and reactivation of embryonic development genes are associated with malignancy in IDH-mutant astrocytoma. *Acta Neuropathol*. 2024;148:50. https://doi.org/10.1007/s00401-024-02811-0

43. Hinz FE, Friedel D, Ippen FM, et al. Loss of global DNA hypermethylation is prognostic in IDH-mutant and 1p/19q-codeleted oligodendrogliomas. *Acta Neuropathol*. 2025;150:56. https://doi.org/10.1007/s00401-025-02963-7

44. Bhatia A, Moreno R, Reiner AS, et al. Tumor volume growth rates and doubling times during active surveillance of IDH-mutant low-grade glioma. *Clin Cancer Res*. 2024;30:106–115. https://doi.org/10.1158/1078-0432.CCR-23-1180

45. Spitzer A, Gritsch S, Nomura M, et al. Mutant IDH inhibitors induce lineage differentiation in IDH-mutant oligodendroglioma. *Cancer Cell*. 2024;42:904–914 e909. https://doi.org/10.1016/j.ccell.2024.03.008

46. Lin B, Wang K, Yuan Y, et al. A novel approach to the analysis of overall survival (OS) as response with progression-free interval (PFI) as condition based on the RNA-seq expression data in the cancer genome atlas (TCGA). *BMC Bioinformatics*. 2024;25:300. https://doi.org/10.1186/s12859-024-05897-1

Neuro-Oncology 2026 28(4) 911–922
https://doi.org/10.1093/neuonc/noaf296
Basic and Translational Investigations